



Cite this: *Nanoscale*, 2015, 7, 5395

High Curie temperature and coercivity performance of $\text{Fe}_{3-x}\text{Cr}_x\text{Se}_4$ nanostructures†

Shao-jie Li, Da Li,* Wei Liu and Zhidong Zhang

Monoclinic $\text{Fe}_{3-x}\text{Cr}_x\text{Se}_4$ nanostructures ($0 \leq x \leq 2.5$) were synthesized using a high-temperature solution chemical method. With increasing the Cr doping, the peak positions in the X-ray diffraction (XRD) patterns of $\text{Fe}_{3-x}\text{Cr}_x\text{Se}_4$ nanostructures slightly shifted to lower 2θ values due to the changes in lattice parameters. Expansions in the unit cell volumes of $\text{Fe}_{3-x}\text{Cr}_x\text{Se}_4$ nanostructures ($x > 0.3$) may have been responsible for enhancing the ferromagnetic (FM) interaction between magnetic ions, which resulted in a significant increase in the Curie temperature (T_C) from 331 K for Fe_3Se_4 to 429 K for FeCr_2Se_4 , distinctly differing from the magnetic properties of the corresponding bulk materials. A room-temperature coercivity (H_C) analysis showed an obvious increase from 3.2 kOe for Fe_3Se_4 to 12 kOe for $\text{Fe}_{2.3}\text{Cr}_{0.7}\text{Se}_4$ nanostructure, but gradually decreased upon further increasing the Cr content.

Received 10th December 2014,
Accepted 9th February 2015

DOI: 10.1039/c4nr07287a

www.rsc.org/nanoscale

Introduction

In the past few decades, magnetic nanostructures have attracted a great deal of interest due to their magnetic properties being different from their bulk counterparts, which offers various opportunities for extensive applications, such as high density data storage and medical equipment. Compared to the top-down physical processes, chemical synthetic methods have been found to be highly effective to synthesize uniform magnetic nanostructures with controlled size and shape by varying the reaction conditions. Through chemical methods, the as-prepared FePt nanoparticles generally take on a disordered face-centered-cubic (FCC) structure without ferromagnetism at the nanoscale;¹ however, after high-temperature salt-matrix annealing, the FCC FePt nanoparticles would convert to the face-centered-tetragonal structure (L1_0), which achieved coercivity values of up to 30 kOe at room temperature with a diameter of 8 nm.² To date, the chemical synthesis has had very limited success in obtaining high coercivity values and high purity specimens of the SmCo and NdFeB nanoparticles. A two-step synthetic approach was developed to prepare nanocrystalline SmCo by high-temperature reductive annealing of the $\text{Co@Sm}_2\text{O}_3$ core/shell nanoparticles in Ca.³ At room temperature, the obtained SmCo nanocrystals showed a coercivity value of 12 kOe. However, the FePt and SmCo nanostructures contained noble metal and rare earth elements and

with that comes the associated problems of cost and resource scarcity. Additionally, the method is very complex and needs to anneal at high temperatures. All these problems demand for a search of new rare earth-free hard magnetic materials.

The iron selenide (FeSe_x) compounds have been studied since the 1950s.^{4–8} They have the NiAs structure similar to pyrrhotite FeS_x , and FeSe_x with the composition between $x = 1.00$ to 1.35 being ferrimagnetic.^{5,6} The crystal structure of Fe_3Se_4 is monoclinic with ordered vacancies of Fe atoms along the b -axis, and the lattice parameters of the unit cell with two chemical units, Fe_3Se_4 , are $a = 0.6208$ nm, $b = 0.3541$ nm, $c = 1.1281$ nm and $\beta = 91.807^\circ$.⁴ The magnetic structure of Fe_3Se_4 has been investigated by high resolution powder neutron diffraction and the magnetic moments have been found to point along the b -axis.⁹ According to the phase diagrams, the $\text{Fe}_{3-x}\text{M}_x\text{Se}_4$ ($\text{M} = \text{Ni}, \text{Co}$ and Cr) systems can form a solid solution with Cr_3S_4 -structures over the entire composition range.¹⁰ The substituted Ni and Co atoms in $\text{Fe}_{3-x}\text{M}_x\text{Se}_4$ have no localized magnetic moment and the ferrimagnetism of Fe_3Se_4 is weakened by Ni and Co substitutions.¹¹ The Curie temperature T_C and the magnetization at a field of 18 kOe for $\text{Fe}_{3-x}\text{M}_x\text{Se}_4$ ($\text{M} = \text{Ni}$ and Co) decrease monotonously with increasing the substitution of Ni and Co, and the ferrimagnetism disappears at about $x = 1.2$ for Ni and $x = 1.8$ for Co. The $\text{Fe}_{3-x}\text{Cr}_x\text{Se}_4$ system shows a ferrimagnetic transition in the susceptibility at around 300 K in the composition range $0 \leq x \leq 1.5$, and the highest T_C of these materials is about 370 K for $x = 0.5$, which is higher than that of Fe_3Se_4 .^{12,13} Fe_3Se_4 nanowire arrays have been investigated by selenizing the precursor Fe nanowires with Se powder,¹⁴ which exhibits a high coercivity performance and a positive magnetoresistance behavior at temperatures below 100 K. Various Fe_3Se_4 nanostructures with shapes from

Shenyang National Laboratory for Materials Science, Institute of Metal Research, Chinese Academy of Sciences, 72 Wenhua Road, Shenyang, 110016, P. R. China.

E-mail: dali@imr.ac.cn

† Electronic supplementary information (ESI) available: EDS compositional analysis. See DOI: 10.1039/c4nr07287a

nanosheets and nanocacti to nanoplatelets showed giant coercivity values up to 40 kOe at 10 K and 4.0 kOe at room temperature.^{15–17} This giant coercivity has been attributed to the uniaxial magnetocrystalline anisotropy of the monoclinic Fe_3Se_4 with ordered cation vacancies.^{15,17} However, the room-temperature coercivity of Fe_3Se_4 nanostructures was one order magnitude smaller than that at 10 K, and the Curie temperature was a bit larger than 300 K, which limits the possible applications of Fe_3Se_4 . In order to enhance the room-temperature magnetic properties of Fe_3Se_4 -based nanostructures, the substitution of Fe atoms by other transition metal elements has been brought forward.^{17,18} With the Co substitution, both the H_C and the T_C of $\text{Fe}_{3-x}\text{Co}_x\text{Se}_4$ nanostructures decreased and the room-temperature coercivity value becomes zero at a Co dopant concentration of $x = 0.2$.¹⁶ By doping Fe-sites with Mn, the magnetization of $\text{Fe}_{3-x}\text{Mn}_x\text{Se}_4$ nanostructures at room temperature increased from 4.84 emu g^{-1} for the $x = 0$ to 7.54 emu g^{-1} for the $x = 0.03$ sample, but the room-temperature coercivity value decreased from 2.74 kOe for Fe_3Se_4 to 1.94 kOe for $\text{Fe}_{2.8}\text{Mn}_{0.2}\text{Se}_4$ and the T_C values were stable.¹⁸

Herein, we synthesized $\text{Fe}_{3-x}\text{Cr}_x\text{Se}_4$ nanostructures by a high-temperature solution chemical method. With the substitution of Fe by Cr ions, the T_C of $\text{Fe}_{3-x}\text{Cr}_x\text{Se}_4$ nanostructures showed a large increase from 331 K for Fe_3Se_4 to about 429 K for FeCr_2Se_4 , which are very different from the magnetic properties of the corresponding bulk materials. Room temperature H_C of $\text{Fe}_{3-x}\text{Cr}_x\text{Se}_4$ nanostructures showed an obvious increase from $x = 0$ to $x = 0.7$, but gradually decreased on further increasing the Cr content. At an optimal Cr dopant of $x = 0.7$, a T_C value of 405 K and the room-temperature H_C value of 12 kOe were obtained, which are considerably larger than those values of 331 K and 3.2 kOe for the undoped Fe_3Se_4 . Heat-treatment at high temperatures can irreversibly change the crystal structures of the as-prepared $\text{Fe}_{3-x}\text{Cr}_x\text{Se}_4$ nanostructures and degrade their magnetic properties. Enhanced T_C and H_C performance of $\text{Fe}_{3-x}\text{Cr}_x\text{Se}_4$ nanostructures may be ascribed to the expanded unit cell volume, enhancing the magnetic interactions.

Experimental

Materials

The $\text{Fe}_{3-x}\text{Cr}_x\text{Se}_4$ nanostructures were synthesized using commercially available reagents. Iron acetylacetonate [$\text{Fe}(\text{acac})_3$, 98%] and oleylamine (OLA, 80%–90%) were supplied by Shanghai Aladdin reagent Co. Ltd. Selenium powder (Se, 99.999%), chromium(III) acetylacetonate [$\text{Cr}(\text{acac})_3$, 98%], hexane (98%), methanol (99.7%) and ethanol (99.7%) were purchased from Sinopharm Chemical Reagent Co. Ltd. (Shenyang, China). All the chemicals were used as received without any further purification.

Synthesis of $\text{Fe}_{3-x}\text{Cr}_x\text{Se}_4$ nanostructures

The synthesis of $\text{Fe}_{3-x}\text{Cr}_x\text{Se}_4$ nanostructures with a series of Fe/Cr mol ratios ($0 \leq x \leq 2.5$) was performed by a high temperature organic solution phase method using a Schlenk line

under air-free conditions and magnetic stirring throughout the entire reaction process. In a typical reaction for the $\text{Fe}_{2.5}\text{Cr}_{0.5}\text{Se}_4$ nanostructure, 1.25 mmol $\text{Fe}(\text{acac})_3$ and 0.25 mmol $\text{Cr}(\text{acac})_3$ were added into 20 ml of OLA in a 250 ml four-neck flask, under a nitrogen flow, which was heated to 180 °C with a 2 °C min^{-1} ramp rate and maintained at 180 °C for 20 min to obtain a mixed solution. At room temperature, 2 mmol Se powder was added into the mixture solution. Under nitrogen flow the mixture was heated to 120 °C and maintained at this temperature for 1 h to remove moisture and air. Then, the temperature was slowly raised to 200 °C with a 2 °C min^{-1} ramp rate and maintained at 200 °C for 1 h. Finally, the solution was heated to 300 °C with a 5 °C min^{-1} ramp rate and maintained at 300 °C for 1 h. After that, the solution was cooled to room temperature by removing the heating source. The $\text{Fe}_{3-x}\text{Cr}_x\text{Se}_4$ nanostructures were precipitated by adding 20 ml ethanol and centrifuged at 6000 rpm for 5 min. The precipitates were rewashed three times with 10 ml of hexane and 20 ml of ethanol.

Characterization methods

The XRD patterns of the nanostructures were collected with the use of a Rigaku D/Max-2400 diffractometer equipped with a Cu K α radiation source ($\lambda = 0.154056$ nm) in the 2θ range of 10°–60° with a step size of 0.02°. The *in situ* high temperature XRD data were obtained on a Bruker D8 Advance diffractometer configured with a tantalum heater as the stage for the powder sample, in which the data were collected by *in situ* heating the samples in a temperature range between 300 K and 450 K under vacuum. The size and morphology of the $\text{Fe}_{3-x}\text{Cr}_x\text{Se}_4$ nanostructures were characterized using a JSM 6301F field-emission scanning electron microscope (SEM) system and a JEOL 2010 transmission electron microscope (TEM). Elemental compositions of the $\text{Fe}_{3-x}\text{Cr}_x\text{Se}_4$ nanostructures were analyzed by an Oxford energy dispersive X-ray spectroscopy (EDX). Magnetic measurements of the as-prepared $\text{Fe}_{3-x}\text{Cr}_x\text{Se}_4$ nanostructures were performed using a vibrating sample magnetometer (VSM) standard option in a physical property measurement system (PPMS) equipped with a superconducting magnet with a maximum magnetic field of 14 T in a temperature range between 5 and 400 K using the standard VSM mode. Compacted $\text{Fe}_{3-x}\text{Cr}_x\text{Se}_4$ pellets were obtained by compacting the as-prepared $\text{Fe}_{3-x}\text{Cr}_x\text{Se}_4$ nanostructures with a diameter of 10 mm using a 1.2 GPa axial pressure with a steel die. The magnetization *versus* temperature curve measurements of the pellets of $\text{Fe}_{3-x}\text{Cr}_x\text{Se}_4$ nanostructures in a temperature range between 300 and 500 K were collected using the VSM with the oven option in a high vacuum state during the oven operation.

Results and discussion

The powder XRD patterns in Fig. 1(a) show that all the $\text{Fe}_{3-x}\text{Cr}_x\text{Se}_4$ nanostructures were in a single phase with the pseudo NiAs-type crystal structure. For $x = 0$, all the XRD peaks

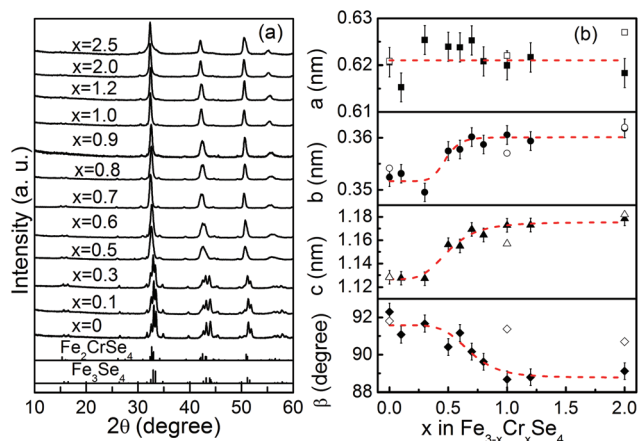


Fig. 1 (a) Powder XRD patterns of the as-prepared $\text{Fe}_{3-x}\text{Cr}_x\text{Se}_4$ nanostructures and the JCPDS XRD cards of Fe_3Se_4 and Fe_2CrSe_4 . (b) lattice parameters (the solid symbols) vs. the Cr content x . The open symbols correspond to the lattice parameters of Fe_3Se_4 , Fe_2CrSe_4 and FeCr_2Se_4 , respectively. The red lines in (b) are guides to the eye.

are in good agreement with the Joint Committee on Powder Diffraction Standards (JCPDS) XRD card (71-2250) for Fe_3Se_4 , which has a monoclinic structure with a space group of $I2/m$ (12) and the unit cell lattice parameters $a = 0.6208$ nm, $b = 0.3541$ nm, $c = 1.1281$ nm and $\beta = 91.807^\circ$. According to the XRD pattern, the grain size of the Fe_3Se_4 nanostructures is about 40 nm as estimated by the full width of the (011) diffraction peak at half maximum, calculated with the Scherrer equation $D = K\lambda/B \cos \theta$, with D being the average size of crystallites, K the dimensionless shape factor assumed to be 0.89 for the spherical shape, $\lambda = 0.15405$ nm the wavelength for the Cu $K\alpha$ radiation source, θ is the Bragg angle and B the full width of the diffraction peak at half maximum located at 2θ . As shown in Fig. 1(a), with a slight substitution for Fe with Cr atoms, the XRD patterns of $\text{Fe}_{3-x}\text{Cr}_x\text{Se}_4$ nanostructures with the Cr content of $x = 0.1$ and 0.3 are quite similar to that of the undoped Fe_3Se_4 nanostructure, but the detailed diffraction data show that the individual peaks are slightly different. As the Cr content was increased, more Fe sites in $\text{Fe}_{3-x}\text{Cr}_x\text{Se}_4$ nanostructures were substituted by Cr atoms and the peak positions of $\text{Fe}_{3-x}\text{Cr}_x\text{Se}_4$ nanostructures with $x \geq 0.5$ significantly shifted to lower 2θ values due to the larger ionic radii of Cr^{2+} (73 pm) and Cr^{3+} (61.5 pm) than those of Fe^{2+} (61 pm) and Fe^{3+} (55 pm). Upon continuously increasing the Cr content, the peak positions gradually approached those of Fe_2CrSe_4 . The lattice parameters of the $\text{Fe}_{3-x}\text{Cr}_x\text{Se}_4$ nanostructures were calculated from the diffraction peaks of (002), (101), (011), (004), (013) and (211) crystal planes using the *UnitCell* program.¹⁹ The calculated lattice parameters of $\text{Fe}_{3-x}\text{Cr}_x\text{Se}_4$ nanostructures and the values extracted from the JCPDS cards of Fe_3Se_4 (71-2250), Fe_2CrSe_4 (89-1966) and FeCr_2Se_4 from ref. 21 are shown in Fig. 1(b). It can be seen that the lattice parameters of $\text{Fe}_{3-x}\text{Cr}_x\text{Se}_4$ nanostructures are almost unchanged with the Cr content of $x \leq 0.3$, which are very close to those for undoped Fe_3Se_4 . The lattice parameter a

has slight changes in all the range of the Cr content in $\text{Fe}_{3-x}\text{Cr}_x\text{Se}_4$ nanostructures, but the lattice parameters b and c obviously increased as the x became larger than 0.5. b and c increase from 0.352 nm and 1.128 nm for the Fe_3Se_4 nanostructure to 0.357 nm and 1.156 nm, respectively, for the $x = 0.5$ nanostructure. The lattice parameters (a , b and c) vs. the Cr content are almost the same as for the $\text{Fe}_{3-x}\text{Cr}_x\text{Se}_4$ solid solution.^{20,21} The angle β of the $\text{Fe}_{3-x}\text{Cr}_x\text{Se}_4$ nanostructures gradually decreased from 91.7° to around 89.1° with increasing the Cr content from $x = 0.3$ to $x = 2$. There is a distinct difference in the lattice parameter β values derived from our present nanostructures and the polycrystalline bulk counterparts, such as Fe_2CrSe_4 and FeCr_2Se_4 .^{20,21} The obvious changes in the angle β for the $\text{Fe}_{3-x}\text{Cr}_x\text{Se}_4$ nanostructures may be ascribed to both the larger ionic radius of Cr than Fe and the small size effect, because the chemical synthesis route for the present nanostructures is very different from the high temperature reaction for polycrystalline bulk materials.²⁰

Nanostructures with interesting morphologies could be obtained using oleylamine as both the solvent and surfactant. Fig. 2(a) shows the SEM image of the undoped Fe_3Se_4 nanoparticles, which are generally a spherical shape, with numerous spikes grown on the surface pointing radially outward, similar to the previous Fe_3Se_4 nanocacti synthesized by Zhang *et al.*¹⁶ The average size of these nanocacti was about 1 μm . With slight substitution for Fe by Cr atoms, the nanostructures

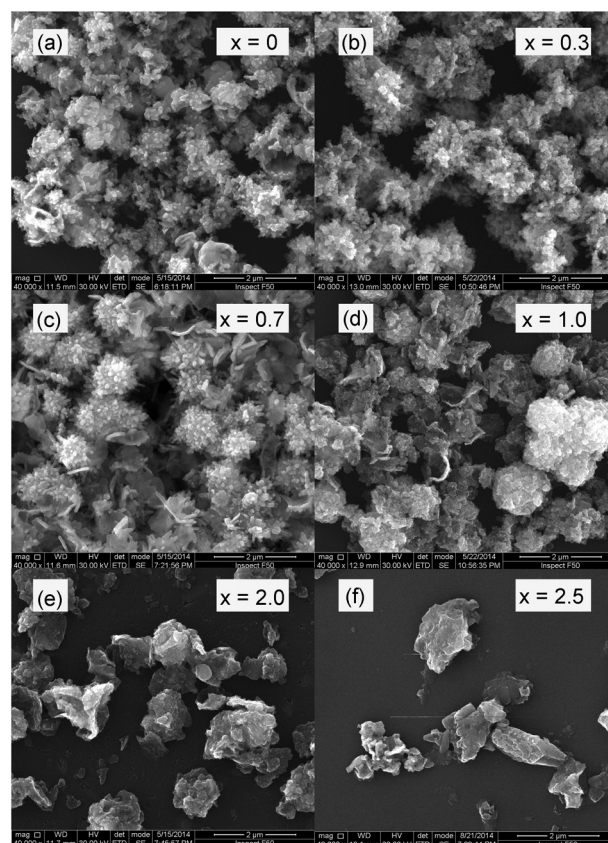


Fig. 2 SEM images for the $\text{Fe}_{3-x}\text{Cr}_x\text{Se}_4$ nanostructures.

with the Cr content of $x = 0.3$ shown in Fig. 2(b) were also in the nanocacti shape. However, the sheet-shape nanostructures appear in Fig. 2(c) as the Cr content was increased up to $x = 0.7$ with a thickness around 50 to 80 nm revealed from the edges of the rolled up nanosheets. The amount of the $\text{Fe}_{3-x}\text{Cr}_x\text{Se}_4$ nanosheets seemed to increase upon increasing the Cr content to $x = 1$ (Fig. 2(d)) and the length of the spikes on the surface of nanocacti became short. With continuous increase in of the Cr content to $x = 2$ and 2.5, Fig. 2(e) and (f), shows that the spikes on the surfaces of the $\text{Fe}_{3-x}\text{Cr}_x\text{Se}_4$ particles disappeared and their shape became irregular with a small increase in the particle size. Compositional line profiles of a $\text{Fe}_{2.3}\text{Cr}_{0.7}\text{Se}_4$ nanocactus and several $\text{Fe}_{2.3}\text{Cr}_{0.7}\text{Se}_4$ nanosheets showed even elemental distributions of Fe, Cr and Se in the nanostructures (Fig. S1(a), ESI†). The relative atomic ratios of Fe, Cr and Se in the $\text{Fe}_{2.3}\text{Cr}_{0.7}\text{Se}_4$ nanostructures were examined by the EDS spectra and are shown in Fig. S1(b) and S1(c).† The Fe/Cr/Se average molar ratio was 32.1/9.2/58.7 for the nanocactus and 30.4/10.5/59.1 for the nanosheets, respectively, and both of them were in good agreement with the composition for the nominal $\text{Fe}_{2.3}\text{Cr}_{0.7}\text{Se}_4$ compound to the detection limit of the instrument.

TEM and HRTEM images in Fig. 3 reveal a more detailed morphology of the $\text{Fe}_{2.3}\text{Cr}_{0.7}\text{Se}_4$ nanocacti. Fig. 3(a) shows that the nanocacti are composed of large numbers of spikes pointing radically outward with a generally spherical shape. The average size of the nanocacti was about 1 μm with the spikes in a diameter between 60 to 80 nm and a length range from 200 to 500 nm. The HRTEM image of $\text{Fe}_{2.3}\text{Cr}_{0.7}\text{Se}_4$ nanocacti shows the spike features growing perpendicularly from their surfaces in detail (Fig. 3(b)) in a single crystal form with a lattice fringe spacing of 0.28 nm, which represents the (202) planes of the monoclinic $\text{Fe}_{2.3}\text{Cr}_{0.7}\text{Se}_4$.

Fig. 4 represents the temperature dependence of the field-cooled (FC) magnetization (M) of the $\text{Fe}_{3-x}\text{Cr}_x\text{Se}_4$ nanostructure measured in a magnetic field of 1 kOe in the temperature range from 400 to 5 K. T_C values of the $\text{Fe}_{3-x}\text{Cr}_x\text{Se}_4$ nanostructures were determined by the point of intersection of the two tangents around the inflection point of the MT curves. The T_C of

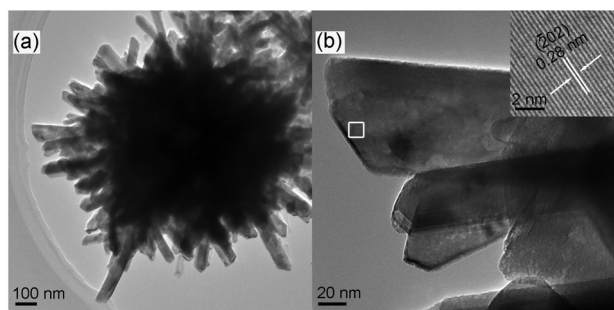


Fig. 3 TEM images of (a) a $\text{Fe}_{2.3}\text{Cr}_{0.7}\text{Se}_4$ nanocactus, (b) the spike feature growing perpendicularly to the surface of the $\text{Fe}_{2.3}\text{Cr}_{0.7}\text{Se}_4$ nanocactus in (a). The inset in (b) shows a HRTEM image of the selected area in a rod with the lattice fringe spacing of 0.28 nm representing the (202) planes of $\text{Fe}_{2.3}\text{Cr}_{0.7}\text{Se}_4$.

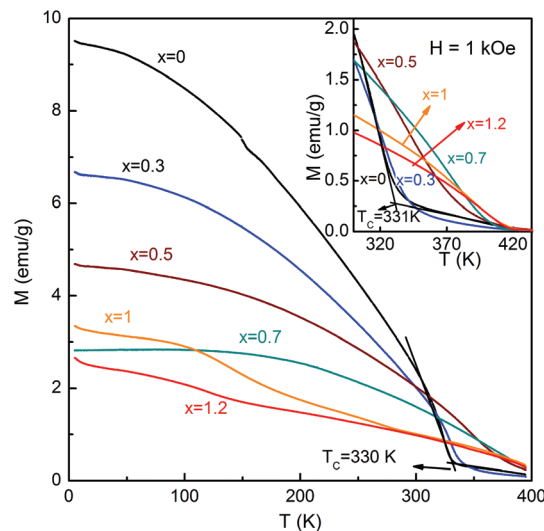


Fig. 4 FC magnetization of the as-prepared $\text{Fe}_{3-x}\text{Cr}_x\text{Se}_4$ nanostructures as a function of temperature. The inset shows the MT curves of the $\text{Fe}_{3-x}\text{Cr}_x\text{Se}_4$ pellets in a heating process from 300 to 450 K.

Fe_3Se_4 nanostructure was found to be 330 K based on Fig. 4 in the FC process, which is in good agreement with the earlier reports.¹⁶ It slightly increased to 343 K for the nanostructure with $x = 0.3$. In the earlier reports of Co doping in Fe_3Se_4 , the T_C of $\text{Fe}_{3-x}\text{Co}_x\text{Se}_4$ nanostructures decreased with increasing Co content, in which the T_C was 290 K for $\text{Fe}_{2.8}\text{Co}_{0.2}\text{Se}_4$ and less than 200 K for Fe_2CoSe_4 .¹⁶ As a result, the hysteresis loops of the $\text{Fe}_{2.8}\text{Co}_{0.2}\text{Se}_4$ and Fe_2CoSe_4 nanostructures showed paramagnetic behavior and the coercivity value decreased to zero at 300 K. With Mn doping ($0 \leq x \leq 0.2$), the T_C of 328 K does not change and the coercivity value at room temperature decreased with the increase in the Mn content.¹⁸ In our present case, beyond $x = 0.3$ ($x \geq 0.5$) the T_C values of the $\text{Fe}_{3-x}\text{Cr}_x\text{Se}_4$ nanostructures have obviously been enhanced and the ferrimagnetic-paramagnetic transitions are not completed at 400 K, which is beyond the measurement range of the standard mode of the VSM measurements. The T_C values of the $\text{Fe}_{3-x}\text{Cr}_x\text{Se}_4$ pellets were measured in a heating process from 300 to 500 K, and then in a magnetic field cooling process from 500 to 300 K using the oven mode of the VSM. The curves measured in the heating process are shown in the inset of Fig. 4. The T_C values of the Fe_3Se_4 and the $\text{Fe}_{2.7}\text{Cr}_{0.3}\text{Se}_4$ nanostructures were determined to be 331 K and 343 K from the compacted pellets in the heating process, which are very close to those obtained from the as-prepared nanostructures in the FC process. However, when the measurement temperature was higher than 400 K, the transition temperatures for the $\text{Fe}_{3-x}\text{Cr}_x\text{Se}_4$ nanostructures obtained from both the heating and cooling processes become different, indicating that some irreversible changes of the $\text{Fe}_{3-x}\text{Cr}_x\text{Se}_4$ nanostructures took place at high temperatures, which are discussed below in detail. Herein, the transition temperatures obtained from the heating process are defined as the T_C of the as-prepared $\text{Fe}_{3-x}\text{Cr}_x\text{Se}_4$ nanostructures, whereas the transition temperatures obtained from

the cooling process are defined as the T_C of the heat-treated $\text{Fe}_{3-x}\text{Cr}_x\text{Se}_4$ nanostructures, which are plotted in Fig. 7(a). On further increasing the Cr doping, the T_C of the as-prepared $\text{Fe}_{3-x}\text{Cr}_x\text{Se}_4$ nanostructures gradually increased from 382 K for $x = 0.5$ to 429 K for $x = 2.5$. It is very surprising that the as-prepared $\text{Fe}_{3-x}\text{Cr}_x\text{Se}_4$ nanostructures ($1 \leq x \leq 2.5$) are ferrimagnetic at room temperature, which differs from their bulk counterparts, with $1.5 \leq x < 3$, which order antiferromagnetically between 170 and 230 K and ferrimagnetically at lower temperatures.¹³ Neutron powder diffraction studies indicated that weak ferrimagnetism occurs in the FeCr_2Se_4 system resulting from a different structural distortion of the Fe and Cr octahedra.²² Moreover, there is a significant enhancement of the T_C of the as-prepared $\text{Fe}_{3-x}\text{Cr}_x\text{Se}_4$ nanostructures in comparison with their bulk counterparts, in which the highest T_C is about 370 K for the $x = 0.5$ compound.¹³ This may be ascribed to the different unit cell lattice parameters between the nanostructures and bulk specimens. The ferrimagnetism of Fe_3Se_4 originates from the ferromagnetically aligned spins within the c -plane coupled antiferromagnetically between adjacent Fe planes with ordered iron vacancies.^{7,23} With increasing Cr content, large changes in the lattice parameters (b , c and β) of the as-prepared $\text{Fe}_{3-x}\text{Cr}_x\text{Se}_4$ nanostructures were observed and are shown in Fig. 1(b), which may have resulted in changes in the distances between the magnetic cations of Fe and Cr, and significantly influenced the ferromagnetic interaction of the spins in the c -plane and antiferromagnetic interaction of the spins between adjacent planes of $\text{Fe}_{3-x}\text{Cr}_x\text{Se}_4$.

Fig. 5 shows the dependence of the unit cell volume (V) of the as-prepared $\text{Fe}_{3-x}\text{Cr}_x\text{Se}_4$ nanostructures on the Cr content. The unit cell volumes of the $\text{Fe}_{3-x}\text{Cr}_x\text{Se}_4$ nanostructures,

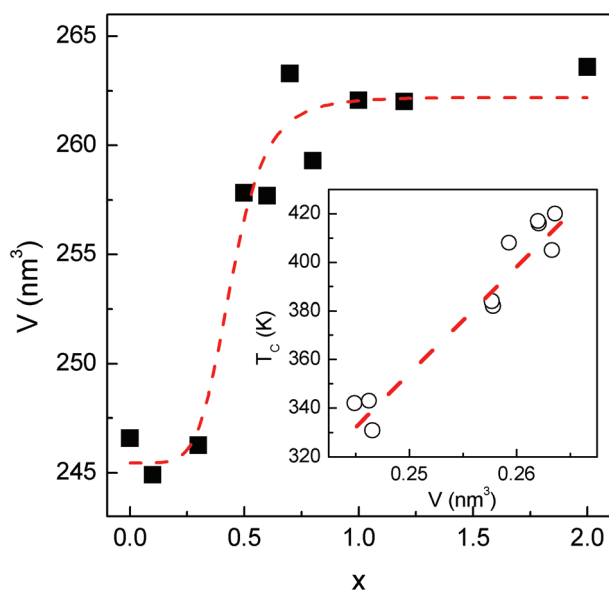


Fig. 5 Cr content dependence of the unit cell volumes of the as-prepared $\text{Fe}_{3-x}\text{Cr}_x\text{Se}_4$ nanostructures. The inset shows a linear fitting between the T_C and the unit cell volume. The lines are guides to the eye.

which were calculated by the formula of $V = abc \sin \beta$, gradually expanded with an increase in the Cr content. Both the T_C (Fig. 7(a)) and the V of the as-prepared $\text{Fe}_{3-x}\text{Cr}_x\text{Se}_4$ nanostructures change slightly for the Cr content $x \leq 0.3$, and increased sharply for $x > 0.3$, and slowly increased beyond $x = 0.8$. The similar behaviors may demonstrate a close relationship between the T_C and the V of the as-prepared $\text{Fe}_{3-x}\text{Cr}_x\text{Se}_4$ nanostructures. The inset in Fig. 5 shows a linear fit between the V and the T_C . In R_2Fe_{17} (R standing for rare-earth elements) type compounds, the T_C decreases strongly under applied pressure²⁴ and increases with increasing the lattice parameters of a and c by the nitrogen atoms occupying the interstitial position in $\text{R}_2\text{Fe}_{17}\text{N}_x$.²⁵ Similarly, the superconducting critical transition temperatures are modulated by the applied pressure and the doping rare-earth atoms in the iron-based superconductors^{26,27} due to the change of the lattice parameters and the internal pressure. The unit cell volumes of the as-prepared $\text{Fe}_{3-x}\text{Cr}_x\text{Se}_4$ nanostructures expanded upon increasing the Cr-doping content, which may change the distances between the magnetic cations of Fe–Fe, Fe–Cr and/or Cr–Cr. According to the Bethe-Slater curve, both the ferromagnetic and the antiferromagnetic interactions between the magnetic ions can be tuned by the distances of the magnetic ions. As a result, a slight increase in the lattice parameter c due to the Cr-doping in Fe_3Se_4 may decrease the antiferromagnetic interaction of magnetic ions between the adjacent planes of $\text{Fe}_{3-x}\text{Cr}_x\text{Se}_4$ nanostructures, and result in the high T_C values.

All of the $\text{Fe}_{3-x}\text{Cr}_x\text{Se}_4$ nanostructures exhibited hard magnetic properties, and the magnetic hysteresis loops at 300 K and 5 K are shown in Fig. 6. The hysteresis loops did not reach saturation even at a high field up to 90 kOe, in which the magnetization of the as-prepared $\text{Fe}_{3-x}\text{Cr}_x\text{Se}_4$ nanostructures increases almost linearly with magnetic fields in the high field range at room temperature. This linear contribution may arise from the spin canting at grain boundaries and particle surfaces.¹⁶ Assuming that the spins in the particle interior remain collinear and reach saturation at the high magnetic field of 90 kOe, we can subtract the paramagnetic component from the magnetic hysteresis to extract the ferrimagnetic part. For the Fe_3Se_4 nanostructures, the saturation magnetization (M_S)

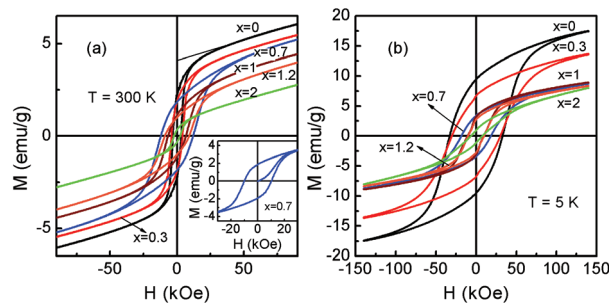


Fig. 6 Hysteresis loops of the as-prepared $\text{Fe}_{3-x}\text{Cr}_x\text{Se}_4$ nanostructures measured at (a) 300 K and (b) 5 K. The inset in (a) shows the magnetization curves of the $\text{Fe}_{2.3}\text{Cr}_{0.7}\text{Se}_4$.

and the remanence magnetization (M_r) are 4.2 emu g^{-1} and 2.2 emu g^{-1} at room temperature, respectively, which increase to 15.9 emu g^{-1} and 9.5 emu g^{-1} at 5 K. Room-temperature M_S of the Fe_3Se_4 nanostructures was slightly different from the values of 5 emu g^{-1} and 4.84 emu g^{-1} from the earlier reports^{16,18} due to a slight difference in the Fe/Se ratio. The dependences of M_S and M_r values on the $\text{Fe}_{3-x}\text{Cr}_x\text{Se}_4$ nanostructures on the Cr content ($0 \leq x \leq 2.5$) had similar tendencies, as shown in Fig. 7(b) and (c). On increasing the Cr doping, the M_S value of the $\text{Fe}_{3-x}\text{Cr}_x\text{Se}_4$ nanostructures progressively decreased due to the weaker localized magnetic moments of the Cr cations compared to the Fe cations, which is similar to the case of the substituted Ni and Co atoms in $\text{Fe}_{3-x}\text{M}_x\text{Se}_4$,¹¹ and/or the antiferromagnetic exchange interaction between Cr ions. Fig. 7(d) shows that the coercivity of the Cr-doped $\text{Fe}_{3-x}\text{Cr}_x\text{Se}_4$ nanostructures at 5 K was almost monotonously reduced with the increasing Cr content. For the Fe_3Se_4 nanostructures, the coercivity value is 33 kOe at 5 K, is in good agreement with earlier value of Fe_3Se_4 nanocacti,¹⁶ while the coercivity value of the $x = 2.5$ nanostructures decreased to 3 kOe, over one order magnitude smaller than that of Fe_3Se_4 . However, it is surprising that the room-temperature coercivity of the as-prepared $\text{Fe}_{3-x}\text{Cr}_x\text{Se}_4$ nanostructures obviously increased with the Cr content from $x = 0$ to $x = 0.7$, and then decreased on further increasing the Cr content. The high room temperature H_C of Cr doped nanostructures may be a result of their different anisotropies and different shape and size of $\text{Fe}_{3-x}\text{Cr}_x\text{Se}_4$ nanostructures. Room-temperature H_C of the $\text{Fe}_{2.3}\text{Cr}_{0.7}\text{Se}_4$ nanostructures is found to be about 12.0 kOe, which is the largest value in the presently reported $\text{Fe}_{3-x}\text{M}_x\text{Se}_4$ (M = Fe, Co and Mn) nanostructures.^{16,18} The inset in Fig. 6(a) shows the magnetization curve of the as-prepared $\text{Fe}_{2.3}\text{Cr}_{0.7}\text{Se}_4$ nanostructures, in which the magnetization is increased slowly at the low field range, and then increases abruptly at the field

around the H_C , indicating the pinning mechanism of the magnetization reversal for the nanostructures.

It has been mentioned before that when the measurement temperature is higher than 400 K, the as-prepared $\text{Fe}_{3-x}\text{Cr}_x\text{Se}_4$ nanostructures experience an irreversible change at high temperatures. As an example, Fig. 8(a) shows the temperature dependence of the magnetization (MT) curve of the $\text{Fe}_{2.3}\text{Cr}_{0.7}\text{Se}_4$ pellet measured in a heating process from 300 K to 500 K under a magnetic field of 1 kOe and Fig. 8(e) shows the MT curve in a field cooling process for comparison. The transition temperature of the as-prepared $\text{Fe}_{2.3}\text{Cr}_{0.7}\text{Se}_4$ nanostructures in the heating curve is 405 K, but 318 K in the cooling process. Fig. 8(b)–(d) present the temperature dependence of the FC magnetization of the $\text{Fe}_{2.3}\text{Cr}_{0.7}\text{Se}_4$ nanostructures from different temperatures of 350 K, 400 K and 450 K, respectively, to 300 K. It is clear that the transition temperatures gradually decreased with an increase in the cooling temperatures, which indicates that the irreversible change of the $\text{Fe}_{2.3}\text{Cr}_{0.7}\text{Se}_4$ nanostructures took place gradually. The inset in Fig. 8 shows the hysteresis loops of the $\text{Fe}_{2.3}\text{Cr}_{0.7}\text{Se}_4$ pellet cooled down from different temperatures to 300 K. The hysteresis loop of the $\text{Fe}_{2.3}\text{Cr}_{0.7}\text{Se}_4$ pellet cooled from 350 K is almost the same as that of as-prepared powder specimen. With increasing the heating temperature, both the M_S and the M_r of the heated $\text{Fe}_{2.3}\text{Cr}_{0.7}\text{Se}_4$ pellet had significantly decreased. It has been reported that the size and dimensions may greatly influence the magnetic properties of Ni nanostructures.²⁸ In the present case, the SEM image in Fig. S2 (ESI[†]) shows that the size and shape of the $\text{Fe}_{2.3}\text{Cr}_{0.7}\text{Se}_4$

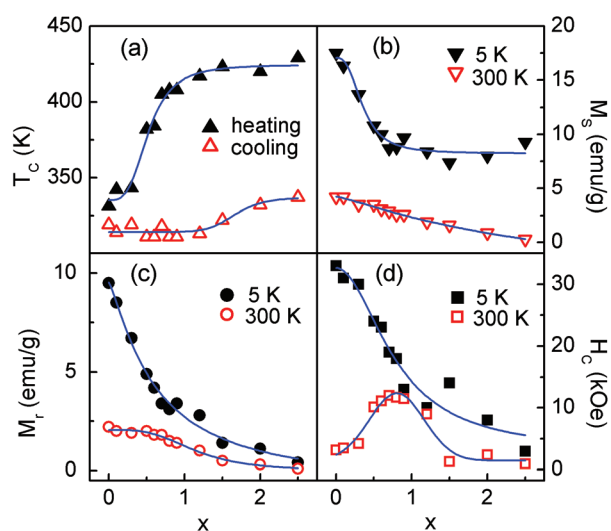


Fig. 7 (a) T_C values of the $\text{Fe}_{3-x}\text{Cr}_x\text{Se}_4$ nanostructures obtained from the heating process (solid symbols) and cooling process (open symbol), (b) M_S , (c) M_r and (d) H_C of the $\text{Fe}_{3-x}\text{Cr}_x\text{Se}_4$ nanostructures measured at 5 K and 300 K. The lines are guides to the eye.

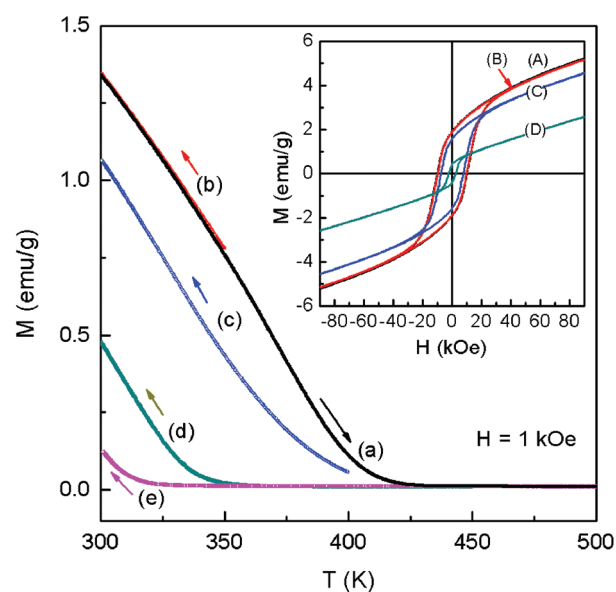


Fig. 8 Temperature dependence of the magnetization of the compacted $\text{Fe}_{2.3}\text{Cr}_{0.7}\text{Se}_4$ pellet measured (a) in a heating process from 300 K to 500 K and in a cooling process from different temperatures of (b) 350 K, (c) 400 K, (d) 450 K and (e) 500 K, respectively, to 300 K. The inset shows the room-temperature hysteresis loops of (A) the $\text{Fe}_{2.3}\text{Cr}_{0.7}\text{Se}_4$ pellet and those cooling from different temperatures of (B) 350 K, (C) 400 K and (D) 450 K.

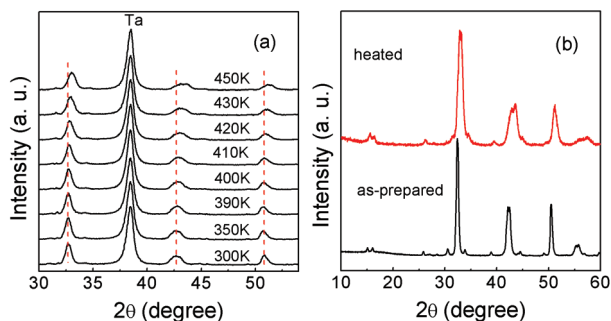


Fig. 9 (a) *In situ* XRD patterns of the $\text{Fe}_{2.3}\text{Cr}_{0.7}\text{Se}_4$ nanostructures recorded at different temperatures. (b) Room-temperature XRD patterns of the as-prepared $\text{Fe}_{2.3}\text{Cr}_{0.7}\text{Se}_4$ nanostructures and the nanostructures after heating at 500 K.

nanostructures underwent slight change after the heating process at 500 K, which suggests that the size and dimensions have no relationship with the change in the magnetic properties of the heated $\text{Fe}_{2.3}\text{Cr}_{0.7}\text{Se}_4$ nanostructures. In order to clarify the influence of the heating temperature on the crystal structure of the $\text{Fe}_{2.3}\text{Cr}_{0.7}\text{Se}_4$ nanostructures, *in situ* high-temperature XRD measurements were carried out at different temperatures and the XRD patterns are shown in Fig. 9(a). As the heating temperature increased from 350 K to 390 K, the XRD patterns are similar to the as-prepared $\text{Fe}_{2.3}\text{Cr}_{0.7}\text{Se}_4$ nanostructures. When the heating temperature was further raised higher than 400 K, the peak positions of the nanostructures shifted to high values of 2θ , whereas the peak position of the Tantalum substrate at $2\theta = 38.5^\circ$ was stable. This indicates that the phase of the as-prepared $\text{Fe}_{2.3}\text{Cr}_{0.7}\text{Se}_4$ nanostructure is stable below 390 K, but becomes unstable at temperatures above 400 K with a contraction in the lattice parameters. After cooling from 500 K, the change in the lattice parameters was maintained, indicating the irreversible change in the crystal structure due to the heating process. Fig. 9(b) shows the difference in the XRD patterns of the as-prepared $\text{Fe}_{2.3}\text{Cr}_{0.7}\text{Se}_4$ nanostructures and the heated nanostructures after the magnetic measurements up to 500 K. The degenerative magnetic parameters, *i.e.* T_C , M_S and H_C , of the heated $\text{Fe}_{3-x}\text{Cr}_x\text{Se}_4$ nanostructures may be attributed to the changed lattice parameters after the heat-treatment.

Conclusions

In conclusion, we synthesized a series of $\text{Fe}_{3-x}\text{Cr}_x\text{Se}_4$ nanostructures with a single phase of the pseudo NiAs-type crystal structure with a high-temperature organic solution phase method. With increasing the Cr content, the peak positions in the XRD patterns of the as-prepared $\text{Fe}_{3-x}\text{Cr}_x\text{Se}_4$ nanostructures slightly shift to lower 2θ values indicating an expansion in the unit cell volume, which tuned the magnetic exchange interaction between the magnetic cations in $\text{Fe}_{3-x}\text{Cr}_x\text{Se}_4$ and resulted in a significant increase in the T_C of the $\text{Fe}_{3-x}\text{Cr}_x\text{Se}_4$ nanostructures. Room-temperature H_C of the

as-prepared $\text{Fe}_{3-x}\text{Cr}_x\text{Se}_4$ nanostructures also showed an obvious increase from 3.2 kOe for Fe_3Se_4 to 12 kOe for the $\text{Fe}_{2.3}\text{Cr}_{0.7}\text{Se}_4$ nanostructures, but gradually decreased with further increase in the Cr content. The T_C is 405 K and the room-temperature H_C reaches 12 kOe for the optimal $\text{Fe}_{2.3}\text{Cr}_{0.7}\text{Se}_4$ nanostructure, which is considerably higher than the values of 331 K and 3.2 kOe for the Fe_3Se_4 nanostructures. These findings suggest that the investigated materials, and possibly materials with other substitutions for Fe in Fe_3Se_4 , could constitute a promising category of alternative low-cost hard-magnetic materials.

Acknowledgements

The work was supported by the National Natural Science Foundation of China under grant no. 51371175 and by the National Basic Research Program (no. 2010CB934603) of China, Ministry of Science and Technology China.

Notes and references

- 1 S. Sun, C. B. Murray, D. Weller, L. Folks and A. Moser, *Science*, 2000, **287**, 1989.
- 2 C. B. Rong, D. Li, V. Nandwana, N. Poudyal, Y. Ding, Z. L. Wang, H. Zeng and J. P. Liu, *Adv. Mater.*, 2006, **18**, 2984.
- 3 Y. Hou, Z. Xu, S. Peng, C. Rong, J. P. Liu and S. Sun, *Adv. Mater.*, 2007, **19**, 3349.
- 4 O. Atsushi and K. Hirakawa, *J. Phys. Soc. Jpn.*, 1956, **11**, 930.
- 5 T. Hirone, S. Maeda and N. Tsuya, *J. Phys. Soc. Jpn.*, 1954, **9**, 496.
- 6 H. Tokutaro and S. Chiba, *J. Phys. Soc. Jpn.*, 1956, **11**, 666.
- 7 K. Hirakawa, *J. Phys. Soc. Jpn.*, 1957, **12**, 929.
- 8 F. Grønvold and E. F. Westrum, *Acta Chem. Scand.*, 1959, **13**, 241.
- 9 A. F. Andresen and B. V. Laar, *Acta Chem. Scand.*, 1970, **24**, 2435.
- 10 H. Akihiko, I. Katsuhiko, I. Kazumichi, U. Yutaka and K. Koji, *Bull. Inst. Chem. Res., Kyoto Univ.*, 1986, **64**, 186.
- 11 K. Kojima, S. Murase, K. Sato and K. Adachi, *J. Phys. Soc. Jpn.*, 1970, **29**, 1642.
- 12 K. Kojima, M. Matsui, K. Sato and K. Adachi, *J. Phys. Soc. Jpn.*, 1970, **29**, 1643.
- 13 G. J. Snyder, T. Caillat and J. P. Fleurial, *Phys. Rev. B: Condens. Matter*, 2000, **62**, 10185.
- 14 D. Li, J. J. Jiang, W. Liu and Z. D. Zhang, *J. Appl. Phys.*, 2011, **109**, 07C705.
- 15 G. Long, H. W. Zhang, D. Li, R. Sabirianov, Z. D. Zhang and H. Zeng, *Appl. Phys. Lett.*, 2011, **99**, 202103.
- 16 H. W. Zhang, G. Long, D. Li, R. Sabirianov and H. Zeng, *Chem. Mater.*, 2011, **23**, 3769.
- 17 J. Wang, H. Duan, X. Lin, V. Aguilar, A. Mosqueda and G. Zhao, *J. Appl. Phys.*, 2012, **112**, 103905.
- 18 M. S. Bishwas, R. Das and P. Poddar, *J. Phys. Chem. C*, 2014, **118**, 4016.

- 19 T. J. B. Holland and S. A. T. Redfern, *Mineral. Mag.*, 1997, **61**, 65.
- 20 G. E. Delgado and V. Sagredo, *Phys. Status Solidi A*, 2004, **201**, 421.
- 21 J. H. Kang, S. J. Kim, B. W. Lee and C. S. Kim, *J. Appl. Phys.*, 2006, **99**, 08F714.
- 22 G. Lamarche, I. Bulyzhenkov, P. Wang, M. Quintero and A. M. Lamarche, *J. Phys. Chem. Solids*, 2008, **69**, 884.
- 23 Y. Takemura, H. Suto, N. Honda, K. Kakuno and K. Saito, *J. Appl. Phys.*, 1997, **81**, 5177.
- 24 M. Brouha, K. H. J. Buschow and A. R. Miedema, *IEEE Trans. Magn.*, 1974, **10**, 182.
- 25 J. M. Coey and H. J. Sun, *Magn. Magn. Mater.*, 1990, **87**, L251.
- 26 H. Takahashi, K. Igawa, K. Arii, Y. Kamihara, M. Hirano and H. Hosono, *Nature*, 2008, **453**, 376.
- 27 J. L. Yang, W. J. Ren, D. Li, W. J. Hu, B. Li and Z. D. Zhang, *Supercond. Sci. Technol.*, 2010, **23**, 025003.
- 28 G. Q. Zhang, T. Zhang, X. L. Lu, W. Wang, J. L. Qu and X. G. Li, *J. Phys. Chem. C*, 2007, **111**, 12663.